

Constraining Solar position and velocity with a Nearby Hypervelocity Star

KOHEI HATTORI,¹ MONICA VALLURI,¹ AND NORBERTO CASTRO^{1,2}

¹*Department of Astronomy, University of Michigan, Ann Arbor, MI, 48104, USA*

²*Leibniz-Institut für Astrophysik Potsdam (AIP), An der Sternwarte 16, 14482, Potsdam, Germany*

ABSTRACT

Gravitational 3-body interaction among binary stars and the supermassive black hole (SMBH) at the center of the Milky Way occasionally ejects a hypervelocity star (HVS) with a velocity of $\sim 1000 \text{ km s}^{-1}$. Due to the ejection location, such a HVS initially has negligible azimuthal angular momentum $L_z \simeq 0 \text{ kpc km s}^{-1}$. Even if the halo is mildly triaxial, L_z of a recently ejected nearby HVS remains negligible, since its flight time from the Galactic Center is too short to accumulate noticeable torque. However, if we make a wrong assumption about the Solar position and velocity, such a HVS would apparently have noticeable non-zero azimuthal angular momentum, due to the wrong reflex motion of the Sun. Conversely, with precise astrometric data for a nearby HVS, we can measure the Solar position and velocity by assuming that the HVS has zero azimuthal angular momentum. Based on this idea, here we propose a method to estimate the Galactocentric distance of the Sun R_0 and the Galactocentric Solar azimuthal velocity V_\odot by using a HVS. We demonstrate with mock data for a nearby HVS candidate that the *Gaia* astrometric data, along with the currently available constraint on V_\odot/R_0 from the proper motion measurement of Sgr A*, can constrain R_0 and V_\odot with uncertainties of $\sim 0.27 \text{ kpc}$ and $\sim 7.8 \text{ km s}^{-1}$ (or fractional uncertainties of 3%), respectively. Our method will be a promising tool to constrain (R_0, V_\odot) , given that *Gaia* is expected to discover many nearby HVSs in the near future.

Keywords: Galaxy: halo – Galaxy: kinematics and dynamics – Galaxy: structure

1. INTRODUCTION

Precise measurement of the position \mathbf{r}_\odot and velocity \mathbf{v}_\odot of the Sun with respect to the Galactic Center (or in the Galactic rest frame) is key to understanding the dynamics of stars in the Milky Way. This is simply because what we observe is the heliocentric position $\mathbf{r}_{\text{helio}}$ and velocity $\mathbf{v}_{\text{helio}}$ of stars with respect to the Sun (or observer); while what we need to know is the 3D position $\mathbf{r} = \mathbf{r}_\odot + \mathbf{r}_{\text{helio}}$ and 3D velocity $\mathbf{v} = \mathbf{v}_\odot + \mathbf{v}_{\text{helio}}$ of stars in the Galactic rest frame in order to describe the motions of stars in the Milky Way. In particular, R_0 (the Galactocentric distance of the Sun) is the most uncertain quantity that characterizes \mathbf{r}_\odot , and V_\odot (azimuthal velocity of the Sun in the Galactic rest frame) is the most uncertain component of \mathbf{v}_\odot , and many authors have proposed and used various methods to estimate these quantities (recent examples include Gillessen et al. 2017, Malhan & Ibata 2017,

and Hayes et al. 2018). Currently, typical fractional uncertainty in R_0 in the literature is $\simeq 5\%$ (see table 3 of Bland-Hawthorn & Gerhard 2016). Given that the astrometric satellite *Gaia* (Gaia Collaboration et al. 2016) will provide accurate measurements of $\mathbf{r}_{\text{helio}}$ and $\mathbf{v}_{\text{helio}}$ of stars, more accurate measurements of R_0 and V_\odot which will enhance the value of *Gaia* data for various other studies of Galactic structure and dynamics.

Currently, one of the most reliable constraints on (R_0, V_\odot) comes from the measurement of the proper motion of Sgr A*, the radio source associated with the supermassive black hole (SMBH) at the very center of the Milky Way. Since Sgr A* is thought to be at rest in the Galactic Center, its proper motion along the Galactic longitude reflects the angular motion of the Sun in the Galactic disc plane. This proper motion was measured with 0.4% precision by Reid & Brunthaler (2004), therefore the ratio V_\odot/R_0 is constrained with 0.4% precision. Given that V_\odot/R_0 is tightly constrained, we only need to add one more independent constraint on (R_0, V_\odot) to measure R_0 and V_\odot individually; and here we propose a

new dynamical method which makes use of hypervelocity stars (HVSs).

Orbits of stars within 0.5 arcsec ($\simeq 0.02$ pc) of the Galactic Center have unambiguously revealed the existence of a central SMBH with a mass of $M = 4 \times 10^6 M_\odot$ (Eisenhauer et al. 2003; Ghez et al. 2008; Gillessen et al. 2009, 2017). Hills (1988) theoretically predicted that when a tightly bound stellar binary passes close enough to this SMBH, the strong tidal force can disrupt the stellar binary. The result of this 3-body interaction is that one of the binary stars (the so-called S-star) is decelerated and gravitationally captured by the SMBH, while the other star attains kinetic energy and escapes from the central region of the Milky Way. The typical ejection velocity of this escaping star, or the HVS, is of the order of 10^3 km s $^{-1}$, exceeding the escape velocity at the Galactic Center. There are several possible definitions for HVSs (Brown 2015), but in this paper we adopt the following definition:

We define HVSs as those stars which are ejected from the center of the Milky Way.

We adopt this definition since our method which we apply to nearby stars is not sensitive to whether or not a star is bound to the Milky Way so long as it is ejected recently (less than a few orbital periods) from the Galactic Center. For example, a short-lived massive star with large space motion is a good candidate for such a star.

After the first discovery of HVS candidate by Brown et al. (2005), about 20 HVS candidates have been reported so far (Brown et al. 2014, 2015; Zheng et al. 2014; Huang et al. 2017). We expect that *Gaia* will discover more HVS candidates (Marchetti et al. 2018), and that some of the HVS candidates will be confirmed to be Galactic Center origin with precise *Gaia* astrometry.

If a HVS is ejected from the Galactic Center by the Hills mechanism, the magnitude of its azimuthal angular momentum $|L_z|$ is much smaller than that of the Sun, $|L_{z,\odot}| = |R_0 V_\odot| \simeq 2 \times 10^3$ kpc km s $^{-1}$. The tidal breakup of a stellar binary near the Galactic Center typically happens at a radius of ~ 30 AU and the ejection velocity of a HVS is typically $\sim 10^3$ km s $^{-1}$. Thus, the typical value of $|L_z|$ of a HVS just after the ejection is $|L_z| \sim 1.5 \times 10^{-4}$ kpc km s $^{-1}$. In the region where the Galactic potential is nearly axisymmetric, the angular momentum L_z is nearly conserved along the orbit. Also, even if the potential is mildly triaxial, L_z is nearly zero for a recently ejected nearby HVS, since it does not have long enough flight time to accumulate torque from the potential and acquire noticeable non-zero L_z . As a result, recently ejected HVSs that are relatively close to the Sun are expected to have negligible L_z . Therefore,

if the heliocentric position $\mathbf{r}_{\text{helio}}$ and velocity $\mathbf{v}_{\text{helio}}$ of a nearby HVS can be accurately measured with astrometric surveys like *Gaia*, we can constrain the position \mathbf{r}_\odot and the velocity of the Sun \mathbf{v}_\odot in the Galactic rest frame, such that the z -component of the angular momentum is zero, i.e.,

$$[(\mathbf{r}_\odot + \mathbf{r}_{\text{helio}}) \times (\mathbf{v}_\odot + \mathbf{v}_{\text{helio}})]_z = 0, \quad (1)$$

for this HVS. To the best of our knowledge, this idea of using HVSs to constrain $(\mathbf{r}_\odot, \mathbf{v}_\odot)$ or (R_0, V_\odot) has never been explored.

In this paper, we provide a theoretical framework to constrain (R_0, V_\odot) from astrometric observations of a single HVS. The outline of this paper is as follows. In Section 2, we explain our Bayesian formulation. In Section 3, we briefly describe a recently discovered HVS candidate, LAMOST-HVS1, and generate *Gaia*-like mock data of this star with the assumption that this star originates from the Galactic Center. In Section 4, we apply our formulation to the mock data and assess the accuracy of our method. In Section 5 we provide some discussion about this method, and Section 6 sums up.

2. FORMULATION

Here we describe our Bayesian formulation to estimate $\theta_G \equiv (R_0, V_\odot)$ by using the astrometric data of a nearby HVS, which is ejected from the Galactic Center.

2.1. Coordinate system

We define a right-hand Cartesian coordinate system centered at the Galactic Center in which (x, y) -plane corresponds to the Galactic plane and z is directed toward the North Galactic Pole. We assume that the Sun is located at $(x, y, z) = (-R_0, 0, z_0)$ and has a velocity of $(v_x, v_y, v_z) = (U_\odot, V_\odot, W_\odot)$. We assume that (z_0, U_\odot, W_\odot) are well determined a priori and (R_0, V_\odot) are to be determined. The uncertainties in z_0 and (U_\odot, W_\odot) are much smaller than those of R_0 and V_\odot , respectively, so our assumption is well justified.

In Section 3, we generate our mock data by assuming $(R_0, z_0) = (8 \text{ kpc}, 0 \text{ pc})$ and $(U_\odot, V_\odot, W_\odot) = (11.1, 240, 7.25) \text{ km s}^{-1}$ (see Schönrich et al. 2010 for U_\odot and W_\odot).

2.2. Observables of a HVS

Let us define the observed 6-dimensional phase-space vector of a (nearby) HVS as

$$\mathbf{q} = (DM, \ell, b, v_{\text{los}}, \mu_{\ell^*}, \mu_b). \quad (2)$$

Here, DM is the distance modulus, (ℓ, b) are respectively the Galactic longitude and latitude (which are assumed

to be determined with infinite precision), v_{los} is the heliocentric line-of-sight velocity, and (μ_{ℓ^*}, μ_b) are respectively the proper motions in the ℓ - and b -directions. Also, we define the true 6-dimensional phase-space vector of this HVS,

$$\mathbf{q}' = (DM', \ell, b, v'_{\text{los}}, \mu'_{\ell^*}, \mu'_b). \quad (3)$$

such that \mathbf{q} and \mathbf{q}' are identical in the limit of no observational error.

In addition, we define a 4-dimensional vector that expresses the observational error given by

$$\boldsymbol{\sigma}_q = (\sigma_{DM}, \sigma_v, \sigma_{\mu_{\ell^*}}, \sigma_{\mu_b}). \quad (4)$$

Here, $(\sigma_{DM}, \sigma_v, \sigma_{\mu_{\ell^*}}, \sigma_{\mu_b})$ are the Gaussian errors in $(DM, v_{\text{los}}, \mu_{\ell^*}, \mu_b)$, respectively. In this paper, we simply assume $\sigma_{\mu_{\ell^*}} = \sigma_{\mu_b} = \sigma_\mu$, but our formulation can be easily generalized to include the correlation coefficient $\rho_{\ell b}$ ($-1 \leq \rho_{\ell b} \leq 1$) in the error distribution of (μ_{ℓ^*}, μ_b) .

2.3. L_z of a HVS

The azimuthal angular momentum $L_z = (xv_y - yv_x)$ of a HVS is essentially zero – since it originates from the Galactic Center. Therefore, the probability distribution function of the true astrometric coordinates $(DM', v'_{\text{los}}, \mu'_{\ell^*}, \mu'_b)$ of a HVS given the parameters $\theta_G = (R_0, V_\odot)$ and the observed direction (ℓ, b) can be simply assumed to be a Dirac Delta function

$$P(DM', v'_{\text{los}}, \mu'_{\ell^*}, \mu'_b | \ell, b, \theta_G) = E \delta(L_z(\mathbf{q}', \theta_G)) \quad (5)$$

with E a constant and

$$L_z(\mathbf{q}', \theta_G) = Av'_{\text{los}} + B\mu'_{\ell^*} + C\mu'_b + D. \quad (6)$$

Here, $A, B, C,$ and D are given by

$$\begin{cases} A = -R_0 \cos b \sin \ell \\ B = kd'(d' \cos b - R_0 \cos \ell) \\ C = kd'R_0 \sin b \sin \ell \\ D = d' \cos b (\cos \ell V_\odot - \sin \ell U_\odot) - R_0 V_\odot, \end{cases} \quad (7)$$

$k = 4.74047 \text{ km s}^{-1} \text{ kpc}^{-1} \text{ mas}^{-1}$ is a constant, and d' is the distance that corresponds to DM' .

Of course, with a detailed model of ejection mechanism of HVSs (e.g., Yu & Madau 2007; Kenyon et al. 2008; Rossi et al. 2017; Marchetti et al. 2018), we can think of more sophisticated probability distribution than equation (5). However, such sophistication may not be helpful for our problem, since we shall use only a single HVS.

2.4. Likelihood function

The probability that a HVS is found at \mathbf{q} in the observable space given the Galactic parameters $\theta_G = (R_0, V_\odot)$ and the observational errors $\boldsymbol{\sigma}_q$ can be expressed as

$$\begin{aligned} P(\mathbf{q} | \theta_G, \boldsymbol{\sigma}_q) &= \int d\mathbf{q}' P(\mathbf{q} | \mathbf{q}', \boldsymbol{\sigma}_q) P(\mathbf{q}' | \theta_G) \quad (8) \\ &= \int d\mathbf{q}' P(\mathbf{q} | \mathbf{q}', \boldsymbol{\sigma}_q) P(DM', v'_{\text{los}}, \mu'_{\ell^*}, \mu'_b | \ell, b, \theta_G) P(\ell, b | \theta_G). \quad (9) \end{aligned}$$

If the observational errors in $(DM, v_{\text{los}}, \mu_{\ell^*}, \mu_b)$ are Gaussian, then we have

$$\begin{aligned} P(\mathbf{q} | \theta_G, \boldsymbol{\sigma}_q) & \quad (10) \\ &= \frac{P(\ell, b | \theta_G) E}{(2\pi)^2 \sigma_{DM} \sigma_v \sigma_\mu \sigma_\mu} \iiint \int_{-\infty}^{\infty} dDM' dv'_{\text{los}} d\mu'_{\ell^*} d\mu'_b \\ & \times \delta(L_z(\mathbf{q}', \theta_G)) \exp \left[-\frac{(DM - DM')^2}{2\sigma_{DM}^2} \right] \\ & \times \exp \left[-\frac{(v_{\text{los}} - v'_{\text{los}})^2}{2\sigma_v^2} - \frac{(\mu_{\ell^*} - \mu'_{\ell^*})^2}{2\sigma_\mu^2} - \frac{(\mu_b - \mu'_b)^2}{2\sigma_\mu^2} \right], \quad (11) \end{aligned}$$

which reduces to

$$\begin{aligned} P(\mathbf{q} | \theta_G, \boldsymbol{\sigma}_q) & \quad (12) \\ &= \frac{P(\ell, b | \theta_G) E}{2\pi \sigma_{DM}} \int_{-\infty}^{\infty} dDM' \exp \left[-\frac{(DM - DM')^2}{2\sigma_{DM}^2} \right] \\ & \times \frac{1}{\sqrt{A^2 \sigma_v^2 + B^2 \sigma_\mu^2 + C^2 \sigma_\mu^2}} \\ & \times \exp \left[-\frac{(Av_{\text{los}} + B\mu_{\ell^*} + C\mu_b + D)^2}{2(A^2 \sigma_v^2 + B^2 \sigma_\mu^2 + C^2 \sigma_\mu^2)} \right]. \end{aligned}$$

In this paper, we assume a Gaussian error distribution for DM for simplicity, but the likelihood function in equation (12) can be easily generalized to a non-Gaussian error distribution for DM (see Appendix A).

2.5. Prior distribution

The proper motion of Sgr A* is observed to be $\mu_{\ell^*, \text{SgrA}} = 6.379 \pm 0.024 \text{ mas yr}^{-1}$ (Reid & Brunthaler 2004). If Sgr A* is at rest at the Galactic Center, this proper motion solely arises from the Solar reflex motion, and we have $V_\odot/R_0 = k\mu_{\ell^*, \text{SgrA}} = 30.24 \pm 0.114 \text{ km s}^{-1} \text{ kpc}^{-1}$. Thus, we adopt a prior distribution for $\theta_G = (R_0, V_\odot)$ of the form

$$P(R_0, V_\odot) dR_0 dV_\odot \propto dR_0 dV_\odot \exp \left[-\frac{(V_\odot/R_0 - \Omega)^2}{2\sigma_\Omega^2} \right]. \quad (13)$$

In our mock analyses in Section 4, we adopt $\Omega = V_\odot/R_0 = 30 \text{ km s}^{-1} \text{ kpc}^{-1}$, and $\sigma_\Omega = 0.116 \text{ km s}^{-1} \text{ kpc}^{-1}$,

Table 1. Basic properties of LAMOST-HVS1

Observed quantities	
(ℓ, b)	$(221.0996^\circ, 35.4072^\circ)$
(α, δ)	$(138.033^\circ, 9.280^\circ)$
B	12.936 ± 0.036
V	13.055 ± 0.009
J	13.357 ± 0.028
H	13.43 ± 0.04
K_s	13.53 ± 0.04
(<i>Gaia</i> DR1) G	14.677731837262346
(Line-of-sight velocity) [†] $v_{\text{los}} \pm \sigma_v$	$611.65 \pm 4.63 \text{ km s}^{-1}$
Estimated quantities	
$\log(g)$	3.5 ± 0.1
T_{eff}	$20000 \pm 1000 \text{ K}$
age τ	$29.91^{+5.28}_{-6.62} \text{ Myr}$
(Current mass) M_*	$9.17^{+1.47}_{-0.73} M_\odot$
(Current radius) R_*	$9.02^{+1.59}_{-1.40} R_\odot$
(Distance modulus) $DM \pm \sigma_{DM}$	16.276 ± 0.569
(Heliocentric distance) d	$18.00^{+5.59}_{-4.03} \text{ kpc}$
Expected <i>Gaia</i> error [‡]	
DR2 parallax error	$\sigma_{\varpi\text{DR2}} = 30 \mu\text{as}$
DR2 proper motion error	$\sigma_{\mu\text{DR2}} = 43 \mu\text{as yr}^{-1}$
Final DR parallax error	$\sigma_{\varpi\text{Final}} = 22.462 \mu\text{as}$
Final DR proper motion error	$\sigma_{\mu\text{Final}} = 11.818 \mu\text{as yr}^{-1}$

[†] Huang et al. (2017) [‡] These quantities are estimated based on the *G*-band magnitude in *Gaia* DR1.

by assuming that the Brownian motion of Sgr A* with respect to the Galactic Center is about 0.2 km s^{-1} (Merriitt et al. 2007).¹

2.6. Bayesian formulation

From Bayes theorem, the posterior probability distribution of θ_G given the observed data \mathbf{q} and information on observational error $\boldsymbol{\sigma}_q$ for HVSs is expressed as

$$P(\theta_G|\mathbf{q}, \boldsymbol{\sigma}_q) = \frac{P(\mathbf{q}|\theta_G, \boldsymbol{\sigma}_q)P(\theta_G)}{P(\mathbf{q}|\boldsymbol{\sigma}_q)}. \quad (14)$$

Here, $P(\theta_G)$ is the prior given in equation (13); $P(\mathbf{q}|\boldsymbol{\sigma}_q)$ is the evidence (which can be regarded as a constant); and the likelihood $P(\mathbf{q}|\theta_G, \boldsymbol{\sigma}_q)$ is given in equation (12).

3. MOCK *Gaia* DATA OF LAMOST-HVS1

Our method of estimating (R_0, V_\odot) from a single HVS can be applied to any HVS. Its performance is determined by the observational error on the position and

velocity of the HVS. Thus, our method is most suited for nearby, bright HVSs for which accurate astrometric data can be obtained. With this regard, the recently discovered nearby HVS candidate, LAMOST-HVS1 (Zheng et al. 2014), is a good test case to examine the accuracy of our method (but see also Section 5.5).

In this section, we briefly review the current knowledge about LAMOST-HVS1. Then we generate mock *Gaia* data for this star with the assumption that it was recently ejected from the Galactic Center. The mock data shall be used in Section 4 to demonstrate the usefulness of our method. A simple test to check whether or not this star originates from the Galactic Center is described in Section 5.2.

3.1. Observed properties of LAMOST-HVS1

The nearby HVS candidate, LAMOST-HVS1, was discovered by Zheng et al. (2014) through the LAMOST survey (Cui et al. 2012; Zhao et al. 2012); and this star is also discussed in Huang et al. (2017). Table 1 shows some of its observed properties (e.g. position and magnitudes) as well as some properties inferred from the spectra. Based on the *G*-band magnitude of this star in *Gaia* Data Release 1 (DR1; Lindegren et al. 2016), we expect that the parallax error and proper motion error in *Gaia* DR2 will be about $\sigma_{\varpi\text{DR2}} = 30 \mu\text{as}$ and $\sigma_{\mu\text{DR2}} = 43 \mu\text{as yr}^{-1}$, respectively. Even if the stellar distance is as close as $d \simeq 13 \text{ kpc}$ (Zheng et al. 2014), the expected fractional error on parallax in *Gaia* DR2 is about $\sigma_{\varpi\text{DR2}}/(1/13 \text{ kpc}) = 0.39$, which is too large to determine the distance based on the parallax only (Bailer-Jones 2015). Therefore, we need to measure stellar distance based on photometric and spectroscopic data.

We re-analyzed the available LAMOST spectra² using a grid of synthetic atmosphere models built using the atmosphere/line formation code FASTWIND (Santolaya-Rey et al. 1997; Puls et al. 2005; Rivero González et al. 2012). The observed spectra are compared with the synthetic FASTWIND grid, retrieving the set of stellar parameters such as $(T_{\text{eff}}, \log g)$ that best reproduce the main chemical transitions in the data (details can be found in Castro et al. 2012). Current stellar radius, age and mass are estimated using the $(T_{\text{eff}}, \log g)$ and the rotating evolutionary tracks published by Ekström et al. (2012). We estimated a distance modulus of $DM = 16.276$ with an uncertainty of $\sigma_{DM} = 0.569$ based on the stellar properties and photometry reported in Table 1, adopting the standard Cardelli et al. (1989) extinction law. The corresponding heliocentric distance to this star is

¹ We note $\sigma_\Omega/\Omega = \sqrt{(0.024/6.379)^2 + (0.2 \text{ km s}^{-1}/V_\odot)^2}$.

² <http://dr3.lamost.org/search>

$d = 18.00_{-4.03}^{+5.59}$ kpc (fractional distance error of $\simeq 27\%$). The heliocentric line-of-sight velocity v_{los} is adopted from [Huang et al. \(2017\)](#).

In the above-mentioned analysis, we assume that this star is an ordinary sub-giant branch star. However, there is a possibility that this star is actually a $9M_{\odot}$ blue straggler. Even if this star is a blue straggler formed out of a mass transfer or merger of binary stars ([Bailyn 1995](#)), we expect that our age (after the formation of a blue straggler) and distance estimates are not seriously affected, as the evolution of blue straggler is quite similar to an ordinary star with the same mass ([Sills et al. 2009](#)).

3.2. Construction of mock Gaia data for LAMOST-HVS1

The currently available proper motion data for LAMOST-HVS1 are associated with large error, and they will be superseded by *Gaia* DR2 proper motion. Therefore, we generate mock *Gaia* proper motion data based on the currently available quantities, $(DM, \sigma_{DM}, \ell, b, v_{\text{los}}, \sigma_v)$. The procedure to generate mock data is described in the following. We note that we generate two sets of mock data: (a) 101 ‘controlled mock data’ of a single mock HVS; and (b) 1000 ‘random mock data’ of a single mock HVS.

3.2.1. Controlled mock data

We generate 101 controlled mock data, each of which is identified by an integer i ($i = 1, 2, \dots, 101$). These controlled mock data are generated in the following manner:

(Step 1) We assume that $R_0 = 8$ kpc, $z_0 = 0$ pc and $(U_{\odot}, V_{\odot}, W_{\odot}) = (11.1, 240, 7.25)$ km s $^{-1}$ in our mock data, and that we know the exact values of $(z_0, U_{\odot}, W_{\odot})$.

(Step 2) Based on the observed values of (DM, v_{los}) and their associated errors of (σ_{DM}, σ_v) , we assign the ‘true’ values of (DM', v'_{los}) . To be specific, we assign

$$DM' = DM + (i - 51)/25 \times \sigma_{DM}, \quad (15)$$

such that the true value of distance modulus increases as a function of i (the mock data ID). By design, $i = 26$ ($i = 76$) corresponds to the case where the true distance modulus DM' is smaller (larger) than the observed value DM by σ_{DM} . Also, $i = 51$ corresponds to the case where the true value DM' happens to be the observed value DM . In this manner, we can easily tell how the systematic error on distance affects the final result. For the true line-of-sight velocity, we randomly draw a velocity from a Gaussian distribution with mean v_{los} and dispersion σ_v :

$$v'_{\text{los}} \sim \mathcal{N}(v_{\text{los}}, \sigma_v). \quad (16)$$

Here, $\mathcal{N}(m, s)$ is a Gaussian distribution with mean m and dispersion s .

(Step 3) Based on the true 4D information of $(DM', \ell, b, v'_{\text{los}})$, we find the orbit that connects the current location and the Galactic Center, such that the star was located at the Galactic Center a few tens of Myr ago. Here, we adopt MWPotential2014 model ([Bovy 2015](#)) as the Galactic potential model. After finding the orbit, we derive the corresponding current ‘true’ proper motion $(\mu'_{\ell*}, \mu'_b)$.

(Step 4) Finally, we add a random Gaussian noise that follows the expected proper motion error distribution for *Gaia* DR2 to the true proper motion $(\mu'_{\ell*}, \mu'_b)$ and obtain the mock *Gaia* proper motion data of $(\mu_{\ell*}, \mu_b)$.

3.2.2. Random mock data

The 1000 random mock data are constructed in the same manner as the controlled mock data (Section 3.2.1), except that we draw the true distance modulus from a Gaussian distribution:

$$DM' \sim \mathcal{N}(DM, \sigma_{DM}), \quad (17)$$

instead of using equation (15) in (step 2).

4. ANALYSES OF MOCK DATA

In this section we apply our Bayesian formulation (Section 2) to our *Gaia*-like mock data described in Section 3.2 to demonstrate how well we can recover the correct values of $(R_0^{\text{correct}}, V_{\odot}^{\text{correct}}) = (8 \text{ kpc}, 240 \text{ km s}^{-1})$ with the astrometric data of a nearby HVS. In these analyses, we use MCMC package of `emcee` ([Foreman-Mackey et al. 2013](#)).

4.1. Results for representative controlled mock data

In order to evaluate how well our method performs, we first focus on three representative controlled mock data with $i = 26, 51$, and 76 . These mock data correspond to the cases where the true value of distance modulus DM' is $DM - \sigma_{DM}$ ($i: 26$), DM ($i: 51$), and $DM + \sigma_{DM}$ ($i: 76$).

Figure 1 shows the two-dimensional posterior distribution of (R_0, V_{\odot}) for these three mock data. In each panel, the blue horizontal or vertical lines correspond to the correct values of $(R_0^{\text{correct}}, V_{\odot}^{\text{correct}})$. In each histogram, the vertical dashed lines indicate either 2.5, 16, 50, 84, or 97.5 percentiles of the posterior distribution. As we can see, there is a tight correlation between R_0 and V_{\odot} , mainly due to the strong prior on V_{\odot}/R_0 . We note that the correct values of R_0 and V_{\odot} are within the central 68 percentiles (between 16 and 84 percentiles) for each of these mock data. The error bars for R_0 and V_{\odot} are about 0.27 kpc and 8 km s $^{-1}$, respectively,

so the fractional uncertainties of these parameters are about 3%. With some additional experiments, we find that these uncertainties can be improved by using a better distance (smaller σ_{DM}) or a better proper motion (smaller σ_μ). Some details are described in Appendix B.

4.2. Results for all the controlled mock data

Given that *Gaia* proper motion error will be as small as $\sigma_{\mu\text{DR2}} = 43 \mu\text{as yr}^{-1}$ even with DR2, the largest source of uncertainty in our method comes from the stellar distance error. Therefore, it is fruitful to see how the difference between the true value of distance modulus DM' and the observed value DM affects our estimation. In our controlled mock data, DM' is designed to be linearly dependent on the integer i (mock data ID). This makes it easier for us to understand how $(DM' - DM)$ affects the posterior distribution.

Figure 2(a) shows the posterior distribution of R_0 for our 101 controlled mock data as a function of i and $(DM' - DM)$. We can see from this figure that the median values of the posterior distributions are located close to the correct value of R_0^{correct} when $-\sigma_{DM} \leq DM' - DM \leq \sigma_{DM}$ (when $26 \leq i \leq 76$). On the other hand, the posterior distributions are shifted toward lower R_0 (resulting in an underestimation of R_0) when $|DM' - DM| > 1.2\sigma_{DM}$ (when $1 \leq i \leq 20$ or $80 \leq i \leq 101$). We note that the posterior distributions are highly broadened for $-\sigma_{DM} \leq DM' - DM \leq -1.64\sigma_{DM}$ ($i = 1-10$), as can be seen from their elongated error bars in Figure 2(a). Fortunately, this region corresponds to $7.16 \leq d'/(kpc) \leq 8.46$, where the fractional distance error based on the *Gaia* DR2 parallax is smaller than 25%. In such a case, we can use the parallax-based distance, which is more reliable than spectroscopic distance.

Figure 2(b) shows the posterior distribution of V_\odot as a function of i . Since we have applied a strong prior on V_\odot/R_0 , the way the posterior distribution of V_\odot depends on i or $(DM' - DM)$ is very similar to that of R_0 .

4.3. Results for random mock data

In order to study the statistical robustness of our method, we analyzed the 1000 random mock data.

First, we looked into the posterior distributions of R_0 . For each random mock datum, we derived the cumulative distribution of R_0 contained in the MCMC posterior distribution and derived the 2.5, 16, 50, 84, and 97.5 percentile values of R_0 . These percentile values of R_0 are denoted as R_{025} , R_{16} , R_{50} , R_{84} , and R_{975} , respectively. We classified the 1000 mock data according to the proximity of the input value, $R_0^{\text{correct}} = 8 \text{ kpc}$,

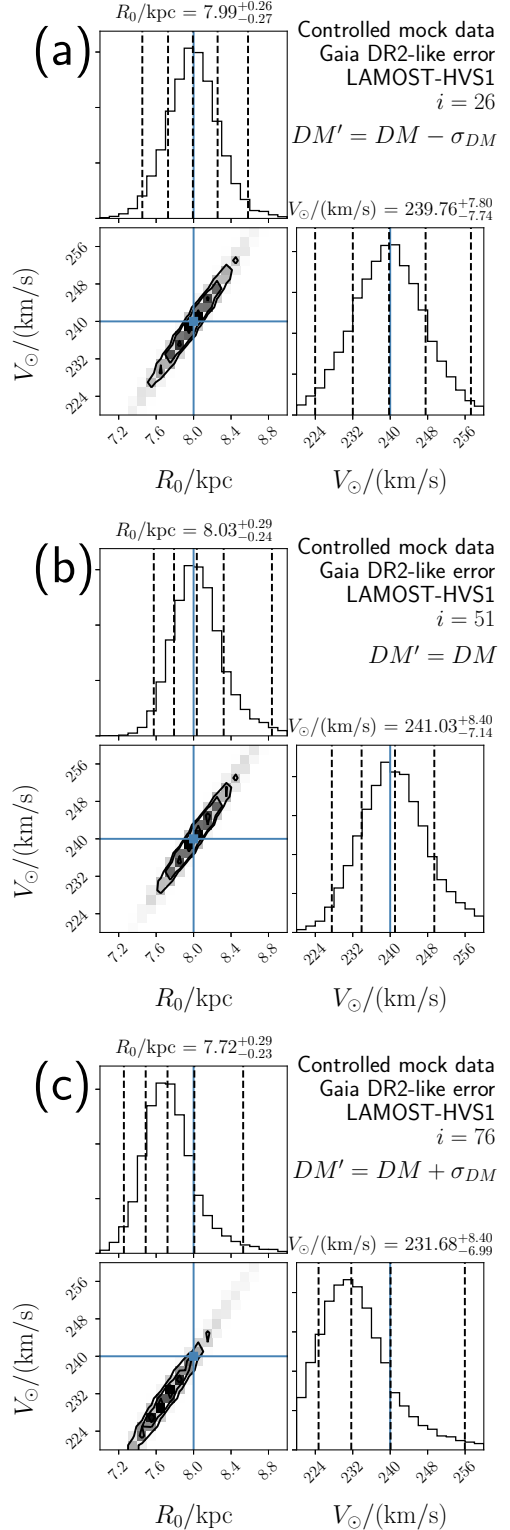


Figure 1. Posterior distributions for three representative controlled mock data of LAMOST-HVS1 with *Gaia* DR2-like proper motion error. (a) Results for mock datum with $i = 26$, where true distance modulus DM' is expressed as $DM' = DM - \sigma_{DM}$. (b) The same figure but with $i = 51$ and $DM' = DM$. (c) The same figure but with $i = 76$ and $DM' = DM + \sigma_{DM}$.

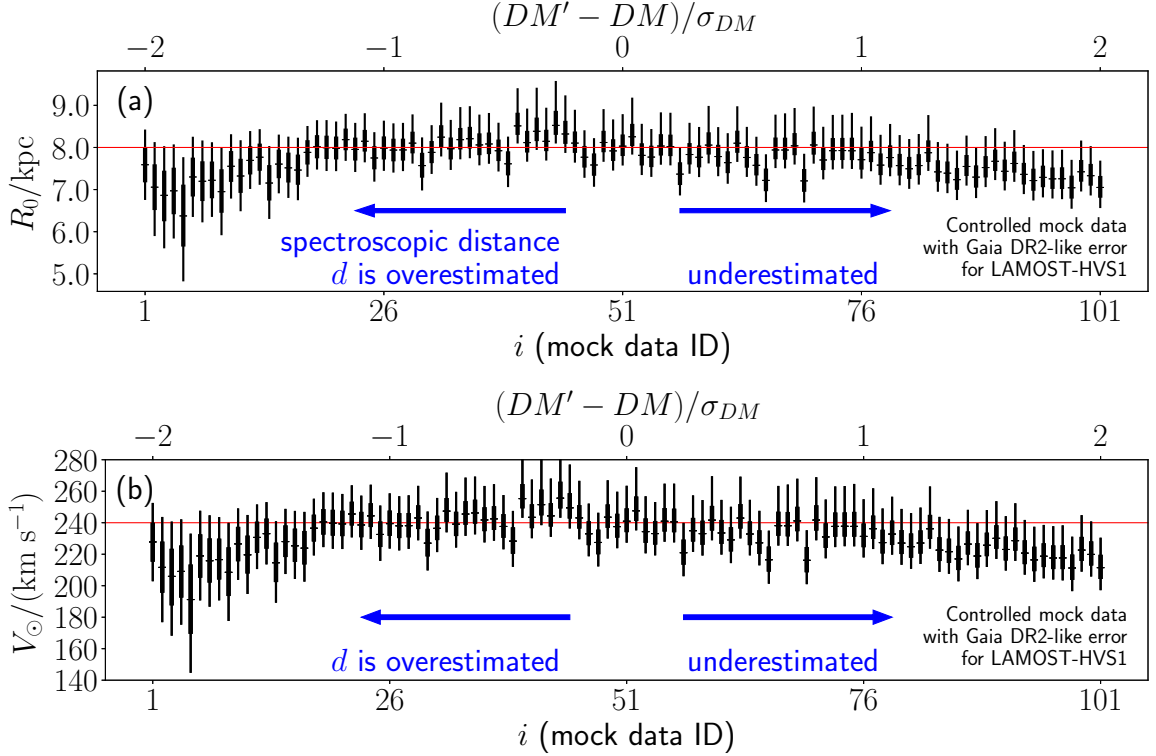


Figure 2. Posterior distributions for 101 controlled mock data of LAMOST-HVS1 with *Gaia* DR2-like proper motion error. Note that the true distance modulus DM' is linearly dependent on i as in equation (15). Namely, the spectroscopic stellar distance d is progressively more overestimated as i decreases from 51 to smaller value; while d is progressively more underestimated as i increases from 51 to larger. (a) The posterior distributions of R_0 . For each value of i , the thin vertical bar covers the 2.5 and 97.5 percentiles of the posterior distribution (central 95 percentiles), the thick vertical bar covers the 16 and 84 percentiles of the posterior distribution (central 68 percentiles), and the horizontal bar shows the 50 percentile (median). The horizontal red line indicates the correct value $R_0^{\text{correct}} = 8$ kpc. (b) The same as in (a), but for the posterior distributions for V_{\odot} . The horizontal red line indicates the correct value $V_{\odot}^{\text{correct}} = 240$ km s $^{-1}$.

and the percentile values such as R_{50} in the posterior distribution, and the results are summarized in Table 2. From this table, we see that 618 ($= 279 + 339$) and 911 ($= 85 + 279 + 339 + 208$) mock data contain the correct value of $R_0^{\text{correct}} = 8$ kpc within their central 68 and 95 percentiles, respectively. We then checked the distribution of R_{50} as shown in Figure 3(a). We found that the median value of R_{50} (median value of 1000 medians) is 7.91 kpc, and the 16 and 84 percentiles of the distribution of R_{50} are respectively 7.48 kpc and 8.18 kpc. The proximity of the median value of R_{50} to R_0^{correct} and the reasonably narrow width of the central 68 percentile of the distribution of R_{50} indicate that our estimation is not seriously biased. Also, we checked the distribution of $(R_{84} - R_{16})/2$, which is a simple measure of the uncertainty associated with our estimation of R_0 . As seen in Figure 3(b), most of the mock data have the uncertainty less than 0.30 kpc and the median value of the uncertainty is 0.27 kpc. Thus, our estimation for R_0 is typically associated with 3% uncertainty. The results in

Figure 3(a)(b) suggest that our method is a promising way of accurately constraining R_0 if LAMOST-HVS1 is ejected from the Galactic Center.

Then we looked into the posterior distributions of V_{\odot} ; and the results are summarized in Table 2. For each posterior distribution of V_{\odot} , we define $V_{025}, V_{16}, V_{50}, V_{84}$, and V_{975} in a similar fashion as in the previous paragraph. We see that 609 and 908 mock data contain the correct value of $V_{\odot}^{\text{correct}} = 240$ km s $^{-1}$ within their central 68 and 95 percentiles, respectively. We then checked the distribution of V_{50} and $(V_{84} - V_{16})/2$ in panels (c) and (d) of Figure 3, respectively. Since we adopt a strong prior on V_{\odot}/R_0 , these histograms are very similar to that of panels (a) and (b) of Figure 3, respectively. The median value of V_{50} is 237.4 km s $^{-1}$, and the 16 and 84 percentiles of the distribution of V_{50} are 224.4 km s $^{-1}$ and 245.3 km s $^{-1}$, respectively. The uncertainty in V_{\odot} , defined by $(V_{84} - V_{16})/2$, is less than 9 km s $^{-1}$ in most cases, and the median value for this uncertainty

Table 2. Posterior distributions of 1000 random mock data

	Number of random mock data
$R_0^{\text{correct}} \leq R025$	15
$R025 < R_0^{\text{correct}} \leq R16$	85
$R16 < R_0^{\text{correct}} \leq R50$	279
$R50 < R_0^{\text{correct}} \leq R84$	339
$R84 < R_0^{\text{correct}} \leq R975$	208
$R975 < R_0^{\text{correct}}$	74
$V_{\odot}^{\text{correct}} \leq V025$	17
$V025 < V_{\odot}^{\text{correct}} \leq V16$	88
$V16 < V_{\odot}^{\text{correct}} \leq V50$	266
$V50 < V_{\odot}^{\text{correct}} \leq V84$	343
$V84 < V_{\odot}^{\text{correct}} \leq V975$	211
$V975 < V_{\odot}^{\text{correct}}$	75

is 7.8 km s^{-1} . These results indicate that V_{\odot} can be estimated with a fractional uncertainty of 3%.

5. DISCUSSION

In our method, a single HVS originating from the Galactic Center is used to constrain (R_0, V_{\odot}) by assuming that $L_z = 0$. However, if this assumption is not strictly valid, our method may result in a biased or wrong estimate on (R_0, V_{\odot}) .

In Section 5.1, we discuss the possible effect from non-zero L_z of a HVS due to the torque from the triaxial halo. In Section 5.2, we discuss a way to judge whether a HVS candidate originates from the Galactic Center. In Section 5.3, we discuss the flight time from the Galactic Center and the stellar age, which is useful to add another clue for the origin of the star. In Section 5.4, we discuss a generalization of our current method to use multiple HVS candidates to minimize the effect of contaminating stars that do not originate from the Galactic Center. Section 5.5 is a note after submission of this paper.

Throughout this Section, for brevity, we use unprimed symbols for true quantities (unlike in previous Sections).

5.1. Effects from a triaxial potential

The main assumption in our method is that a HVS ejected from the Galactic Center has negligible azimuthal angular momentum, $L_z \simeq 0$. However, even if a HVS originates from the Galactic Center, its L_z may deviate from zero as it travels in a triaxial halo (Gnedin et al. 2005).³ In order to investigate the effect of triaxial potential on a recently ejected nearby HVS

(such as an early B-type massive main-sequence HVS), we perform some additional tests.

First, we slightly modify the model potential of MW-Potential2014 (Bovy 2015), such that its spherical dark matter halo is deformed to have a triaxial shape while keeping the dark matter density at the Solar position and the axisymmetric baryonic potential unchanged. We assume that the density distribution of the dark matter is stratified on concentric ellipsoids with principle axes aligned with Cartesian coordinates (x, y, z) defined in Section 2.1. Then we vary the ratio of intermediate-axis to the major-axis (b/a) and the ratio of minor-axis to the major-axis (c/a) and generate mock data of LAMOST-HVS1 in the same manner as in Section 3.2. We find that even when the dark matter halo is maximally triaxial with $(b/a, c/a) = (0.79, 0.5)$, $|L_z|$ is typically smaller than 40 kpc km s^{-1} .

This result means that recently ejected LAMOST-HVS1-like nearby HVSs typically have $|L_z|$ which is less than 2% of that of the Sun, since their flight time is too short to acquire large angular momentum from the triaxial halo. Therefore, even in this worst scenario of maximally triaxial dark matter halo within the current location of LAMOST-HVS1 (at the Galactocentric radius of $r \simeq 24 \text{ kpc}$), the assumption of $L_z = 0$ is expected to result in less than 2% systematic error in our estimation of (R_0, V_{\odot}) . In order to confirm this rough estimation, we analyze these mock data generated in the deformed triaxial potential by using our method (in which $L_z = 0$ is assumed) and by assuming *Gaia* DR2-like proper motion error. We compared the results of representative mock data and found that introducing maximally triaxial dark matter halo results in a systematic change in R_0 by 0.11 kpc or in V_{\odot} by 3 km s^{-1} . This systematic error corresponds to a fractional error of $\sim 1.4\%$, which is consistent with the above-mentioned rough estimate (smaller than 2%). We have also confirmed that the systematic error due to the triaxial halo is smaller for less triaxial cases. Given that the random error in our method is of the order of 3%, the systematic error due to the triaxial halo (smaller than 1.4%) is probably negligible as long as the *Gaia* DR2 proper motion is available.

5.2. Diagnosis based on the proper motion

If we mistakenly apply our method to a star that was not ejected from the Galactic Center (e.g., those stars that were ejected from a binary system in the stellar

³ We note that the z -component of the torque from the stellar disk is zero if it is axisymmetric. Thus, stellar disk's torque only

changes (L_x, L_y) and does not change L_z if it is axisymmetric. The torque from the Galactic bar is negligible for recently ejected HVSs, since HVSs quickly escape from the bar region.

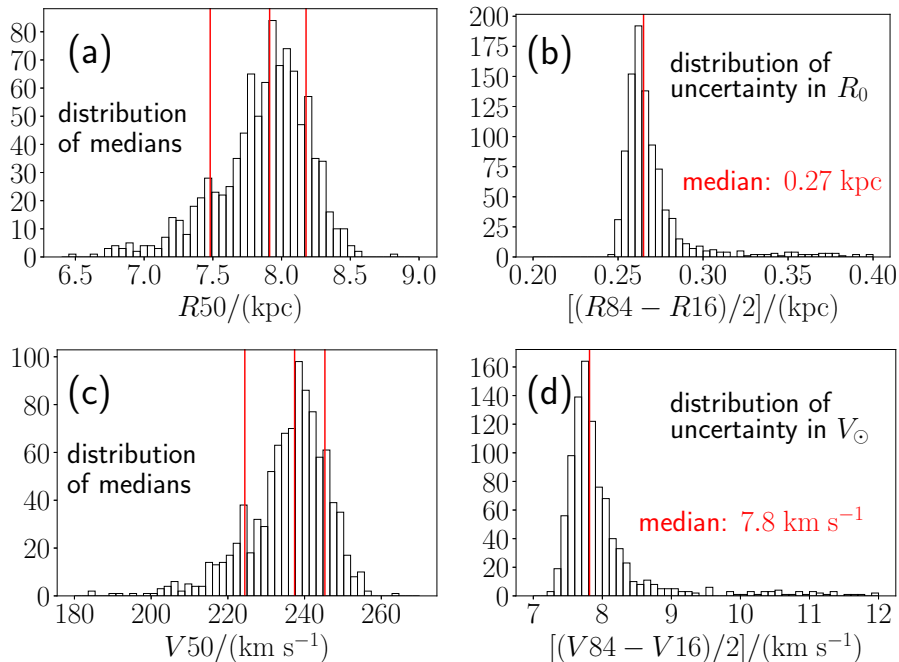


Figure 3. Statistical properties of the posterior distributions of R_0 and V_\odot for our 1000 random mock data. (a) Histogram of $R50$ (the median value of the posterior distribution of R_0 for each datum). The red lines correspond to the 16, 50, and 84 percentiles of the distribution of $R50$. (b) Histogram of the uncertainty in R_0 . The median value of the uncertainty (shown in red) is 0.27 kpc. (c) The same as (a), but for $V50$ (posterior median for V_\odot). (d) Histogram of the uncertainty in V_\odot . The median value of the uncertainty (shown in red) is 7.8 km s⁻¹. These results show that the uncertainties in (R_0, V_\odot) are typically about 3% in our method. Histograms (a) and (c); as well as (b) and (d) look similar to each other due to the strong prior in V_\odot/R_0 .

disc after the supernova explosion of the binary companion, Blaauw 1961; or those stars that were ejected from the Large Magellanic Cloud, Edelmann et al. 2005; Boubert & Evans 2016; Lennon et al. 2017), we would obtain unreliable estimates of (R_0, V_\odot) . In order to judge whether a given HVS candidate originates from the Galactic Center, the proper motion data is very useful.

Let us suppose that we are interested in a HVS candidate in the halo region of the Milky Way which is as young as 100 Myr (or younger); and for which $(\ell, b, v_{\text{los}})$ are measured with high precision. These properties are satisfied by some of the currently known HVS candidates, including LAMOST-HVS1.

In this case, if the star was really ejected from the Galactic Center, there is a tight relationship between the true distance and the true proper motion, $(d, \mu_{\ell*}, \mu_b)$. To be specific, given some reasonable assumptions of the potential of the Milky Way as well as the position and velocity of the Sun, the true proper motion $(\mu_{\ell*}, \mu_b)$ is a well-defined function of the true distance d .

As an illustration, we calculate the expected proper motion of LAMOST-HVS1. Here, we assume a simpler potential model than in Section 3, and allow the Solar

position and velocity to vary within the observed ranges of parameters. Namely, we assume a flexible Galactic potential model of the form

$$\Phi(R, z) = \frac{1}{2}v_0^2 \ln [R_c^2 + R^2 + z^2/q^2]. \quad (18)$$

The Solar position and velocity are described by $R_0 = 8.33 \pm 0.35$ kpc (Gillessen et al. 2009), $V_\odot = (30.24 \pm 0.116 \text{ km s}^{-1} \text{ kpc}^{-1})R_0$ (Reid & Brunthaler 2004; we take into account the Brownian motion of SgrA* as in Section 2.5), $z_0 = -0.9 \pm 0.9$ pc (Bovy 2017), and $(U_\odot, W_\odot) = (11.1^{+0.69}_{-0.75}, 7.25^{+0.37}_{-0.36})$ km s⁻¹ (Schönrich et al. 2010). The parameters for the potential are assumed to be $v_0 = V_\odot - (12.24^{+0.47}_{-0.47} \text{ km s}^{-1})$ (Schönrich et al. 2010), $q = 0.9 \pm 0.1$ (cf. Koposov et al. 2010), and $R_c = 0.01R_0$. In order to evaluate the probability distribution of the expected proper motion of LAMOST-HVS1, first we randomly draw 1000 pairs of values of (d, v_{los}) from the associated error distribution. Then for each (d, v_{los}) , we randomly draw a set of parameters $(R_0, z_0, U_\odot, V_\odot, W_\odot, v_0, q)$ from the associated error distribution and calculate the true proper motion $(\mu_{\ell*}, \mu_b)$. Based on the 1000 realizations of $(\mu_{\ell*}, \mu_b)$, we estimate the probability density

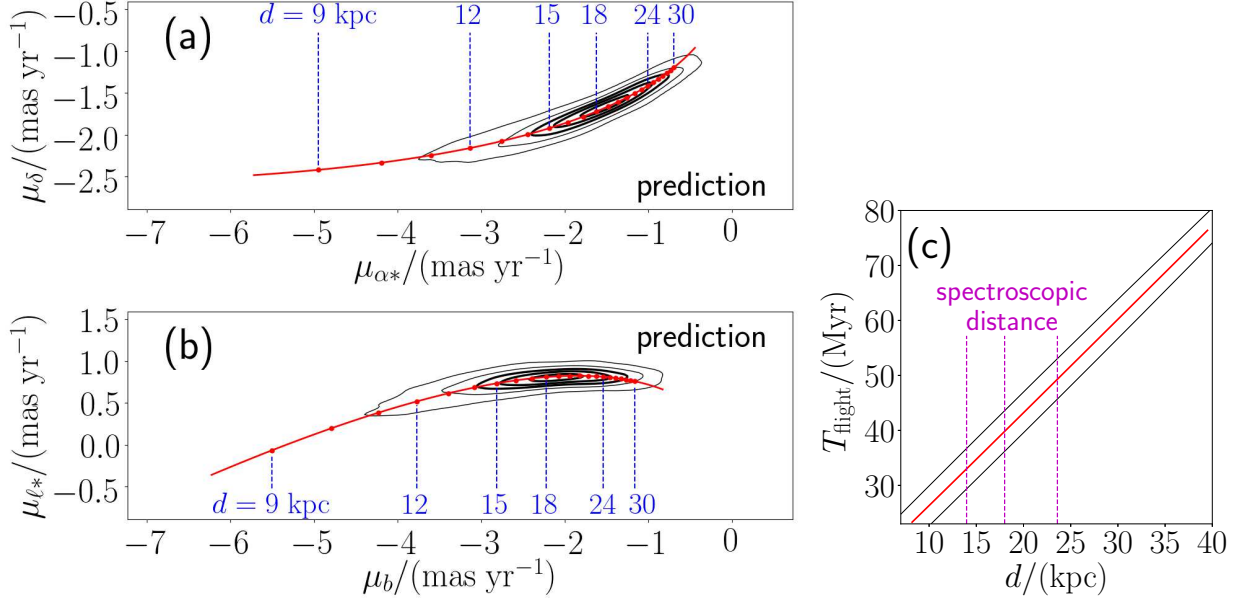


Figure 4. (a) Predicted 2D proper motion ($\mu_{\alpha^*}, \mu_\delta$) of LAMOST-HVS1 based on the assumption that this star originates from the Galactic Center. In estimating proper motion, we use $d = 18.00^{+5.59}_{-4.03}$ kpc and $v_{\text{los}} = 611.65 \pm 4.63$ km s⁻¹; and we consider the uncertainties in the Solar position/velocity and the Galactic potential. The outer thin contours enclose 90% and 70% of the probability; while the inner thick contours enclose 50%, 30%, and 10% of the probability. The red line indicates the predicted proper motion for the fiducial model where only d is varied. Along this red line, the prediction for $d/\text{kpc} = 9, 10, \dots, 30$ are shown with red dots. (b) The same as panel (a) but for the 2D proper motion (μ_b, μ_{ℓ^*}). (c) The predicted flight time of LAMOST-HVS1 since its ejection at the Galactic Center as a function of heliocentric distance. Here, the red line shows the prediction for the fiducial model, while the black lines represents 90% uncertainty for this prediction. Our spectroscopic distance estimate of $d = 18.00^{+5.59}_{-4.03}$ kpc is represented by the three vertical dotted lines in magenta.

distribution of the true proper motion as shown in Figure 4(a)(b). The outer thin contours enclose 90% and 70% of the probability; while the inner thick contours enclose 50%, 30%, and 10% of the probability. We also show the result for a fiducial model with a solid red line, in which we fix $v_{\text{los}} = 611.65$ km s⁻¹ and $(R_0, z_0, U_\odot, V_\odot, W_\odot, v_0, q) = (8.33 \text{ kpc}, -0.9 \text{ pc}, 11.1 \text{ km s}^{-1}, 251 \text{ km s}^{-1}, 7.25 \text{ km s}^{-1}, 239.66 \text{ km s}^{-1}, 0.9)$, and we vary only the heliocentric distance d . We have confirmed that adopting a more realistic potential model of MWPotential2014 (Bovy 2015) instead of our fiducial model results in very similar prediction about the proper motion, which justifies our use of a simpler potential model.

We can clearly see from Figure 4(a)(b) that the allowed proper motion vector is highly restricted if we require the star to be recently ejected from the Galactic Center (cf. Gnedin et al. 2005). We note that the uncertainty in *Gaia* DR2 proper motion is expected to be as small as $\sigma_{\mu_{\text{DR2}}} = 43 \mu\text{as yr}^{-1}$, and it is much smaller than the width of the contours in μ_δ or μ_{ℓ^*} direction. Thus, we can determine whether LAMOST-HVS1 originates from the Galactic Center by checking whether the *Gaia* proper motion is consistent with our prediction.

5.3. Diagnosis based on the flight time and stellar age

In some cases, the origin of a HVS candidate can be inferred from the required flight time for the star to travel from the Galactic Center to the current location. As an illustration, Figure 4(c) shows the expected flight time of LAMOST-HVS1 as a function of its heliocentric distance d , assuming that this star was ejected from the Galactic Center. Here, the red solid line corresponds to the fiducial model, while the black lines enclose 90% of the 1000 random orbits generated in Section 5.2. If we adopt the median spectroscopic distance of $d = 18$ kpc, the expected flight time in the fiducial potential model is 40 Myr. This fiducial flight time of 40 Myr is larger than our best-fit stellar age of 30 Myr (see Table 1). If we adopt the these quantities at face values (neglecting the uncertainties in stellar age, distance, and the Galactic potential), it may suggest that this star is not ejected from the Galactic Center (possibly ejected from the stellar disc). However, if LAMOST-HVS1 is not an ordinary sub-giant branch star but a blue straggler, the origin of this star can still be attributed to an ejection event at the Galactic Center. For example, suppose that a triple stellar system is disrupted by the SMBH at the Galactic

Center to produce a hypervelocity binary system of two stars with $4.5M_{\odot}$ each (Fragione & Gualandris 2018). If such binary stars merge together ~ 10 Myr after the ejection, a $9M_{\odot}$ hypervelocity blue straggler can be formed. When this blue straggler becomes 30 Myr old, this star reaches the current location of the LAMOST-HVS1 but its orbital flight time is 40 Myr (see similar arguments in Edelmann et al. 2005; Lu et al. 2007; Perets 2009; Brown et al. 2015 for another HVS candidate, HVS3). In any case, the orbit of LAMOST-HVS1 will provide a lot of useful information regarding its formation.

5.4. Use of multiple HVS candidates

More than 20 HVS candidates have been published so far. Most of them are compiled in Brown et al. (2014, 2015), and some candidates based on LAMOST survey (Zheng et al. 2014; Huang et al. 2017) have been added to the list (cf. see Marchetti et al. 2017 for more recently claimed candidates based on *Gaia* DR1).

Our current method makes use of a single HVS candidate to estimate (R_0, V_{\odot}) . Unfortunately, the heliocentric distances to the known candidates are typically larger than 20 kpc, and the current spectroscopic distance error and the expected astrometric error with *Gaia* are too large for us to extract useful information on (R_0, V_{\odot}) from each individual star, probably except for a handful of nearby HVS candidates including LAMOST-HVS1.⁴ Therefore, our current method cannot be applied to most of the other currently known HVS candidates. However, each of these distant HVS candidates does have some information about (R_0, V_{\odot}) . In the forthcoming paper, we will generalize our method to use an ensemble of HVS candidates (some of which are allowed to be non-HVS contaminants) to constrain (R_0, V_{\odot}) . This generalized method will be very powerful if *Gaia* discovers more HVS candidates with accurate astrometric data within ~ 20 kpc from the Sun (cf. see Marchetti et al. 2018) and if reliable line-of-sight velocity (and spectroscopic distance) for these new candidates are obtained with the ground-based surveys such as *Gaia*-ESO (Gilmore et al. 2012), RAVE (Kunder et al. 2017), GALAH (Martell et al. 2017), 4MOST (de Jong et al. 2016), WEAVE (Dalton et al. 2012) and DESI (DESI Collaboration et al. 2016).

5.5. A note after submission of this paper

After this paper first appeared on April 23, 2018, *Gaia* Data Release 2 (DR2) revealed that LAMOST-HVS1

⁴ Some HVS candidates in Marchetti et al. (2017) can be also used, although their spectroscopic distances are rather uncertain.

is not a HVS ejected from the Galactic Center, but a hyper-runaway star ejected from the stellar disk of the Milky Way (Hattori et al. 2018). This means that we cannot apply our method to the data for LAMOST-HVS1 to constrain (R_0, V_{\odot}) . However, since the main aim of this paper is to introduce a new method to measure (R_0, V_{\odot}) , the true nature of LAMOST-HVS1 is not essential.

Also, after this paper first appeared, Gravity Collaboration et al. (2018) estimated $R_0 = 8.127 \pm 0.031$ kpc (with an accuracy of 0.4%), by using a General Relativistic effect of the orbit of ‘S2’ star near the Sgr A*.

6. CONCLUSION

In this paper, we have explored a new Bayesian method to constrain R_0 and V_{\odot} with astrometric information for a HVS ejected from the Galactic Center, by noting that the azimuthal angular momentum L_z of such a HVS is essentially zero.

In order to demonstrate the usefulness of this method, we created mock *Gaia* data for LAMOST-HVS1, a recently discovered nearby HVS candidate, by assuming that this star is ejected from the Galactic Center (but see also Section 5.5). Based on the mock analyses, we found that the *Gaia* DR2 data and a modest spectroscopic distance (with $\simeq 27\%$ error) would be sufficient to constrain R_0 with 0.27 kpc uncertainty and V_{\odot} with 7.8 km s^{-1} uncertainties if we additionally use the proper motion data of the Sgr A* (Reid & Brunthaler 2004) as an independent constraint. The 3% uncertainty in R_0 (and V_{\odot}) is significantly better than most of the other methods with typically 5% uncertainty (see Table 3 of Bland-Hawthorn & Gerhard 2016).

Our method will perform better with a more accurate distance estimate to LAMOST-HVS1 and with a better proper motion measurement (see Appendix B; but see also Section 5.5). This may include a sophisticated Bayesian stellar distance estimate combined with *Gaia* parallax information (Schneider et al. 2014; Anderson et al. 2017; Leistedt & Hogg 2017), the *twin* method explored by Jofré et al. (2015, 2017) (finding an even closer star that is spectroscopically similar to the target star – LAMOST-HVS1 in our case – to determine its absolute magnitude), more future *Gaia* proper motion data (the end-of-mission *Gaia* error will be a few times better than the near-future *Gaia* DR2 error), or the distant future astrometric observations by a Theia-like satellite (The Theia Collaboration et al. 2017).

Our method of constraining R_0 and V_{\odot} with a single HVS can be applied to any nearby HVSs, implying that finding more HVSs with *Gaia* (Marchetti et al. 2017, 2018) will be very helpful. In the forthcoming paper, we

discuss how to use more than one nearby HVSSs (within ~ 20 kpc) to better constrain R_0 and V_\odot .

ACKNOWLEDGMENTS

The authors thank the stellar halos group at the Department of Astronomy, University of Michigan for stimulating discussions. M.V. and K.H. are supported by NASA-ATP award NNX15AK79G. We thank Anthony Brown for making `PyGaia` available.⁵ We thank

Foreman-Mackey for making `emcee` available.⁶ Guoshoujing Telescope (the Large Sky Area Multi-Object Fiber Spectroscopic Telescope LAMOST) is a National Major Scientific Project built by the Chinese Academy of Sciences. Funding for the project has been provided by the National Development and Reform Commission. LAMOST is operated and managed by the National Astronomical Observatories, Chinese Academy of Sciences.

REFERENCES

- Anderson, L., Hogg, D. W., Leistedt, B., Price-Whelan, A. M., & Bovy, J. 2017, arXiv:1706.05055
- Bailer-Jones, C. A. L. 2015, *PASP*, 127, 994
- Bailyn, C. D. 1995, *ARA&A*, 33, 133
- Blaauw, A. 1961, *BAN*, 15, 265
- Bland-Hawthorn, J., & Gerhard, O. 2016, *ARA&A*, 54, 529
- Boubert, D., & Evans, N. W. 2016, *ApJL*, 825, L6
- Bovy, J. 2015, *ApJS*, 216, 29
- Bovy, J. 2017, *MNRAS*, 470, 1360
- Brown, W. R., Geller, M. J., Kenyon, S. J., & Kurtz, M. J. 2005, *ApJL*, 622, L33
- Brown, W. R., Geller, M. J., & Kenyon, S. J. 2014, *ApJ*, 787, 89
- Brown, W. R. 2015, *ARA&A*, 53, 15
- Brown, W. R., Anderson, J., Gnedin, O. Y., et al. 2015, *ApJ*, 804, 49
- Cardelli, J. A., Clayton, G. C., & Mathis, J. S. 1989, *ApJ*, 345, 245
- Castro, N., Urbaneja, M. A., Herrero, A., et al. 2012, *A&A*, 542, A79
- Cui, X.-Q., Zhao, Y.-H., Chu, Y.-Q., et al. 2012, *Research in Astronomy and Astrophysics*, 12, 1197
- Dalton, G., Trager, S. C., Abrams, D. C., et al. 2012, *Proc. SPIE*, 8446, 84460P
- de Jong, R. S., Barden, S. C., Bellido-Tirado, O., et al. 2016, *Proc. SPIE*, 9908, 99081O
- DESI Collaboration, Aghamousa, A., Aguilar, J., et al. 2016, arXiv:1611.00036
- Edelmann, H., Napiwotzki, R., Heber, U., Christlieb, N., & Reimers, D. 2005, *ApJL*, 634, L181
- Ekström, S., Georgy, C., Eggenberger, P., et al. 2012, *A&A*, 537, A146
- Eisenhauer, F., Schödel, R., Genzel, R., et al. 2003, *ApJL*, 597, L121
- Foreman-Mackey, D., Hogg, D. W., Lang, D., & Goodman, J. 2013, *PASP*, 125, 306
- Fragione, G., & Gualandris, A. 2018, *MNRAS*, 475, 4986
- Gaia Collaboration, Prusti, T., de Bruijne, J. H. J., et al. 2016, *A&A*, 595, A1
- Ghez, A. M., Salim, S., Weinberg, N. N., et al. 2008, *ApJ*, 689, 1044-1062
- Gillessen, S., Eisenhauer, F., Trippe, S., et al. 2009, *ApJ*, 692, 1075
- Gillessen, S., Plewa, P. M., Eisenhauer, F., et al. 2017, *ApJ*, 837, 30
- Gilmore, G., Randich, S., Asplund, M., et al. 2012, *The Messenger*, 147, 25
- Gnedin, O. Y., Gould, A., Miralda-Escudé, J., & Zentner, A. R. 2005, *ApJ*, 634, 344
- Gravity Collaboration, Abuter, R., Amorim, A., et al. 2018, *A&A*, 615, L15
- Hattori, K., Valluri, M., Castro, N., et al. 2018, arXiv:1810.02029
- Hayes, C. R., Law, D. R., & Majewski, S. R. 2018, arXiv:1809.07654
- Hills, J. G. 1988, *Nature*, 331, 687
- Huang, Y., Liu, X.-W., Zhang, H.-W., et al. 2017, *ApJL*, 847, L9
- Jofré, P., Mädler, T., Gilmore, G., et al. 2015, *MNRAS*, 453, 1428
- Jofré, P., Traven, G., Hawkins, K., et al. 2017, *MNRAS*, 472, 2517
- Kenyon, S. J., Bromley, B. C., Geller, M. J., & Brown, W. R. 2008, *ApJ*, 680, 312-327
- Koposov, S. E., Rix, H.-W., & Hogg, D. W. 2010, *ApJ*, 712, 260
- Kunder, A., Kordopatis, G., Steinmetz, M., et al. 2017, *AJ*, 153, 75
- Leistedt, B., & Hogg, D. W. 2017, *AJ*, 154, 222
- Lennon, D. J., van der Marel, R. P., Ramos Lerate, M., O'Mullane, W., & Sahlmann, J. 2017, *A&A*, 603, A75

⁵ Available at <https://github.com/agabrown/PyGaia>

⁶ Available at <https://github.com/dfm/emcee>

- Lindegren, L., Lammers, U., Bastian, U., et al. 2016, *A&A*, 595, A4
- Lu, Y., Yu, Q., & Lin, D. N. C. 2007, *ApJL*, 666, L89
- Malhan, K., & Ibata, R. A. 2017, *MNRAS*, 471, 1005
- Marchetti, T., Rossi, E. M., Kordopatis, G., et al. 2017, *MNRAS*, 470, 1388
- Marchetti, T., Contigiani, O., Rossi, E. M., et al. 2018, *MNRAS*,
- Martell, S. L., Sharma, S., Buder, S., et al. 2017, *MNRAS*, 465, 3203
- Merritt, D., Berczik, P., & Laun, F. 2007, *AJ*, 133, 553
- Perets, H. B. 2009, *ApJ*, 698, 1330
- Puls, J., Urbaneja, M. A., Venero, R., et al. 2005, *A&A*, 435, 669
- Reid, M. J., & Brunthaler, A. 2004, *ApJ*, 616, 872
- Rivero González, J. G., Puls, J., Massey, P., & Najarro, F. 2012, *A&A*, 543, A95
- Rossi, E. M., Marchetti, T., Cacciato, M., Kuiack, M., & Sari, R. 2017, *MNRAS*, 467, 1844
- Santolaya-Rey, A. E., Puls, J., & Herrero, A. 1997, *A&A*, 323, 488
- Schönrich, R., Binney, J., & Dehnen, W. 2010, *MNRAS*, 403, 1829
- Schneider, F. R. N., Langer, N., de Koter, A., et al. 2014, *A&A*, 570, A66
- Sills, A., Karakas, A., & Lattanzio, J. 2009, *ApJ*, 692, 1411
- The Theia Collaboration, Boehm, C., Krone-Martins, A., et al. 2017, arXiv:1707.01348
- Yu, Q., & Madau, P. 2007, *MNRAS*, 379, 1293
- Zhao, G., Zhao, Y.-H., Chu, Y.-Q., Jing, Y.-P., & Deng, L.-C. 2012, *Research in Astronomy and Astrophysics*, 12, 723
- Zheng, Z., Carlin, J. L., Beers, T. C., et al. 2014, *ApJL*, 785, L23

APPENDIX

A. NON-GAUSSIAN ERROR DISTRIBUTION FOR THE DISTANCE MODULUS

In the main text of this paper, we assumed that the error distribution for $(DM, v_{\text{los}}, \mu_{\ell^*}, \mu_b)$ are all Gaussian. However, the assumption of Gaussian error for DM is not very realistic. In general, the likelihood in equation (12) can be expressed as

$$P(\mathbf{q}|\theta_G, \boldsymbol{\sigma}_q) = \frac{P(\ell, b|\theta_G)E}{\sqrt{2\pi}} \int_{-\infty}^{\infty} dDM' \frac{P(DM'|DM, \boldsymbol{\sigma}_q)}{\sqrt{A^2\sigma_v^2 + B^2\sigma_\mu^2 + C^2\sigma_\mu^2}} \exp\left[-\frac{(Av_{\text{los}} + B\mu_\ell + C\mu_b + D)^2}{2(A^2\sigma_v^2 + B^2\sigma_\mu^2 + C^2\sigma_\mu^2)}\right], \quad (\text{A1})$$

where $P(DM'|DM, \boldsymbol{\sigma}_q)$ is the probability that the true distance modulus is DM' given the observed distance modulus DM and any associated error information $\boldsymbol{\sigma}_q$.

B. PERFORMANCE OF OUR METHOD AS A FUNCTION OF OBSERVATIONAL UNCERTAINTIES

In the main text, we present the analyses of mock *Gaia* data for LAMOST-HVS1, by assuming that the spectroscopic distance modulus error is $\sigma_{DM} = 0.569$ (distance error of $\simeq 27\%$) and *Gaia* DR2-like proper motion error is $\sigma_{\mu\text{DR2}} = 43 \mu\text{as yr}^{-1}$. Here we demonstrate how the inferred values of (R_0, V_\odot) depend on the quality of data.

We adopt five values for distance modulus uncertainty of $\sigma_{DM} = 0.109, 0.218, 0.328, 0.440, \text{ and } 0.555$, which roughly correspond to fractional distance uncertainty of $\sigma_d/d = 5, 10, 15, 20, \text{ and } 25\%$. Also, we adopt two values for proper motion uncertainty of $\sigma_\mu = \sigma_{\mu\text{DR2}}$ and $\sigma_{\mu\text{Final}}$ (see Table 1).

For each pair of $(\sigma_{DM}, \sigma_\mu)$, we generate 100 random mock data in the same manner as in Section 3.2.2. We analyze each mock datum, and derive $R50$ and $V50$ from the posterior distributions (as defined in Section 4.3).

Figure 5 shows the distribution of 100 values of $R50$ and $V50$ as a function of σ_d/d for $\sigma_\mu = \sigma_{\mu\text{DR2}}$ (panels (a) and (c)) and for $\sigma_\mu = \sigma_{\mu\text{Final}}$ (panels (b) and (d)). Since the result for $R50$ and $V50$ behaves in a similar manner due to the strong prior on V_\odot/R_0 , it is sufficient to look at the results for $R50$ only – panels (a) and (b). Figure 5(a) suggests that, with *Gaia* DR2-like proper motion error, we can estimate R_0 better (with smaller uncertainty) by improving σ_d/d up to 15%; but improving distance uncertainty will hardly benefit the result beyond that point since the uncertainty in R_0 is limited by the proper motion error in *Gaia* DR2 at $\sigma_d/d < 15\%$. By comparing panels (a) and (b) of Figure 5, we see that the improved proper motion error in the *Gaia* final data release (which is better than that in DR2 by a factor of a few), will be beneficial to better estimate R_0 for a fixed value of σ_d/d . For example, if the heliocentric distance to LAMOST-HVS1 can be estimated with 15% fractional error, the proper motion information from *Gaia* final data release can constrain R_0 (and V_\odot) with $\simeq 1.7\%$ error under the assumption that LAMOST-HVS1 is ejected from the Galactic Center. These results encourage us to seek for better measurements of the distance to LAMOST-HVS1 or any other HVS candidates to rigorously estimate the position and velocity of the Sun, (R_0, V_\odot) .

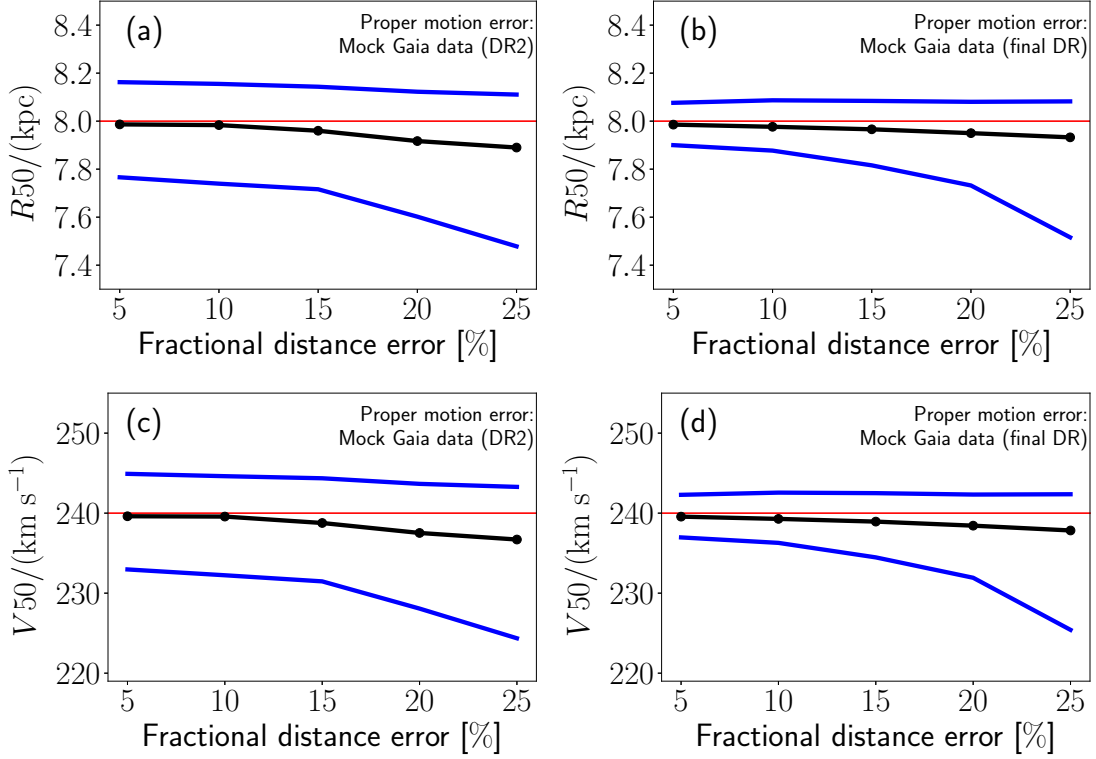


Figure 5. Predicted performance of our method to estimate (R_0, V_\odot) by using mock LAMOST-HVS1 star with *Gaia*-like proper motion error. (a) The distribution of median value R_{50} of the posterior distribution of R_0 as a function of fractional heliocentric distance error to LAMOST-HVS1 when *Gaia* DR2-like proper motion error is considered. The middle black line indicates the median value of the distribution of R_{50} , while the blue lines indicate the range of central 68 percentiles of the distribution of R_{50} . The red horizontal line corresponds to the correct input value of R_0^{correct} . (b) The same as in (a), but the *Gaia* final data release-like proper motion error is considered instead. (c) The same as in (a), but showing the distribution of V_{50} . The red horizontal line corresponds to the correct input value of V_\odot^{correct} . (d) The same as in (c), but the *Gaia* final data release-like proper motion error is considered instead. We can see the shrinkage of the uncertainties in R_0 and V_\odot as heliocentric distance error becomes smaller. For the *Gaia* DR2-like data, improvements in R_0 or V_\odot is only prominent up to 15% distance error, while for the *Gaia* final data release-like data, improvements is prominent up to 10% distance error.